

## Supplement Materials

### Coordination-Layer Engineering of Pt Single Atoms on h-BN for Propane Dehydrogenation via a p-Band Descriptor Validated by Multiscale Modeling and Knowledge-Informed Machine Learning

HuiJie Wang<sup>a#</sup>, WeiHang Xu<sup>a#</sup>, XiaoYing Sun<sup>a\*</sup>, JiaXin Sun<sup>a</sup>, Ji Qi<sup>a</sup>, Zhen Zhao<sup>a,b</sup>, Bo Li<sup>a\*</sup>

<sup>a</sup>Institute of Catalysis for Energy and Environment, College of Chemistry and Chemical Engineering, Shenyang Normal University, Shenyang 110034, China

<sup>b</sup>State Key Laboratory of Heavy Oil Processing, China University of Petroleum, Beijing, 102249, China

Corresponding Authors:

\* B. Li: boli@synu.edu.cn

\* X.Y. Sun: sunxiaoying78@163.com

#: equally contribution

**Table S1.** Summary of Key Calculated Properties for Pt/V<sub>B</sub> and Pt/V<sub>N</sub> series Catalysts.

Catalyst	Formation Energy, E <sub>f</sub> (eV)	Bader Charge on Pt, Pt(e)	Average p-band (eV)	Average ICOHP (eV)
Pt/V <sub>B</sub>	0.17	+0.68	-4.626	-3.43
Pt/V <sub>B</sub> -C1	0.21	+0.59	-3.791	-3.56
Pt/V <sub>B</sub> -C2	0.26	+0.44	-2.775	-3.57
Pt/V <sub>B</sub> -C3	0.31	+0.33	-1.986	-3.69
Pt/V <sub>N</sub>	0.17	-1.04	-4.151	-3.23
Pt/V <sub>N</sub> -C1	0.19	-0.74	-4.317	-3.23
Pt/V <sub>N</sub> -C2	0.21	-0.24	-4.773	-3.87
Pt/V <sub>N</sub> -C3	0.24	-0.18	-5.435	-3.9

**Table S2.** Hyperparameter Search Space and Optimal Configuration

Model	Hyperparameter Search Space	B-series Optimal	N-series Optimal
PhysFormer	hidden $\in \{16, 32\}$ , depth $\in \{2, 3\}$ , dropout $\in \{0, 0.2\}$ , lr $\in \{3e-3, 5e-3\}$ , wd $\in$ $\{1e-3, 2e-2\}$	hidden=32, depth=3, dropout=0.2, lr=5e- 3, wd=1e-3	hidden=16, depth=2, dropout=0, lr=3e-3, wd=2e-2
RandomForest	n_estimators $\in \{100,$ 200, 300}, max_depth $\in \{3, 4, 5,$ 6}	n_estimators=300, max_depth=4	n_estimators=200, max_depth=5
XGBoost	max_depth $\in \{2, 3,$ 4}, learning_rate $\in$ $\{0.01, 0.05, 0.1\}$ , n_estimators=500	max_depth=4, lr=0.01	max_depth=2, lr=0.01
Ridge	$\alpha = 1.0$ , with additional inverse temperature feature 1/T	—	—

**Table S3. Model Performance Comparison**

Series	Model	Train R <sup>2</sup>	LOCO R <sup>2</sup>
B	PhysFormer	0.98	<b>0.94</b>
B	RandomForest	0.99	0.90
B	XGBoost	0.99	0.86
B	Ridge	0.02	-0.01
N	PhysFormer	0.99	<b>0.96</b>
N	RandomForest	0.99	0.95
N	XGBoost	0.99	0.93
N	Ridge	0.00	0.00

**Table S4. Parameters for RMG input files.**

Property	Value
Temperatures	600-1000 K
nSim	7
Pressure	1 bar
Active site	Pt
Surface site density	$2.943 \times 10^{-5}$ , mol/m <sup>2</sup>
Specific surface area	$1 \times 10^5$ m <sup>2</sup> m <sup>-3</sup>
toleranceMoveToCore, $\epsilon_{\text{core}}$	$1 \times 10^{-1}$
toleranceKeepInEdge, $\epsilon_{\text{core}}$	0
terminationRateRatio, $\epsilon_{\text{rate}}$	$1 \times 10^{-7}$
toleranceInterruptSimulation,	$1 \times 10^8$
maximumSurfaceSites	1
maximumEdgeSpecies	500000
Initial composition	10 % C <sub>3</sub> H <sub>8</sub> , 10 % H <sub>2</sub> , 80 % N <sub>2</sub>
Initial coverage	Vacant site fraction = 1.0

**Table S5.** Calculated first C-H bond activation energy barriers ( $E_a$ ) for propane and corresponding Turnover Frequencies (TOFs) at 800 K and 1 bar on catalysts with different local coordination environments.

Catalyst Model	Pt Substitution Site	No. of Neighboring C Atoms	$E_a$ (eV)	TOF (s <sup>-1</sup> )
Pt/V <sub>B</sub>	B	0	0.31	11.59
Pt/V <sub>B</sub> -C1	B	1	0.53	9.49
Pt/V <sub>B</sub> -C2	B	2	0.70	6.94
Pt/V <sub>B</sub> -C3	B	3	0.96	4.93
Pt/V <sub>N</sub>	N	0	0.86	5.57
Pt/V <sub>N</sub> -C1	N	1	0.67	7.60
Pt/V <sub>N</sub> -C2	N	2	0.61	8.58
Pt/V <sub>N</sub> -C3	N	3	0.55	9.53

**Table S6.** Gibbs free energy for activation of the first C-H bond in each catalyst at 800 K.

Catalyst Model	Gibbs free energy (eV)
Pt/V <sub>B</sub>	0.2
Pt/V <sub>B</sub> -C1	0.45

Pt/V <sub>B</sub> -C2	0.46
Pt/V <sub>B</sub> -C3	0.79
Pt/V <sub>N</sub>	0.61
Pt/V <sub>N</sub> -C1	0.53
Pt/V <sub>N</sub> -C2	0.44
Pt/V <sub>N</sub> -C3	0.34

**Table S7.** LOCO cross-validation performance of PhysFormer and baseline models on the B and N catalyst series. Train R<sup>2</sup> and Test R<sup>2</sup> are bootstrap-resampled means; 95% CI denotes the bootstrap confidence interval.

Series	Model	Train R <sup>2</sup>	Train 95% CI	Test R <sup>2</sup>	Test 95% CI
B	PhysFormer	0.98	[0.95, 0.98]	0.94	[0.87, 0.97]
B	RandomForest	0.99	[0.97, 0.99]	0.90	[0.79, 0.95]
B	XGBoost	0.99	[0.98, 0.99]	0.86	[0.67, 0.96]
B	Ridge	0.02	[-0.30, 0.09]	-0.01	[-0.34, 0.09]
N	PhysFormer	0.99	[0.98, 0.99]	0.96	[0.94, 0.98]
N	RandomForest	0.99	[0.98, 0.99]	0.95	[0.90, 0.98]
N	XGBoost	0.99	[0.98, 0.99]	0.93	[0.88, 0.97]
N	Ridge	0.004	[-0.34, 0.05]	0.001	[-0.35, 0.04]

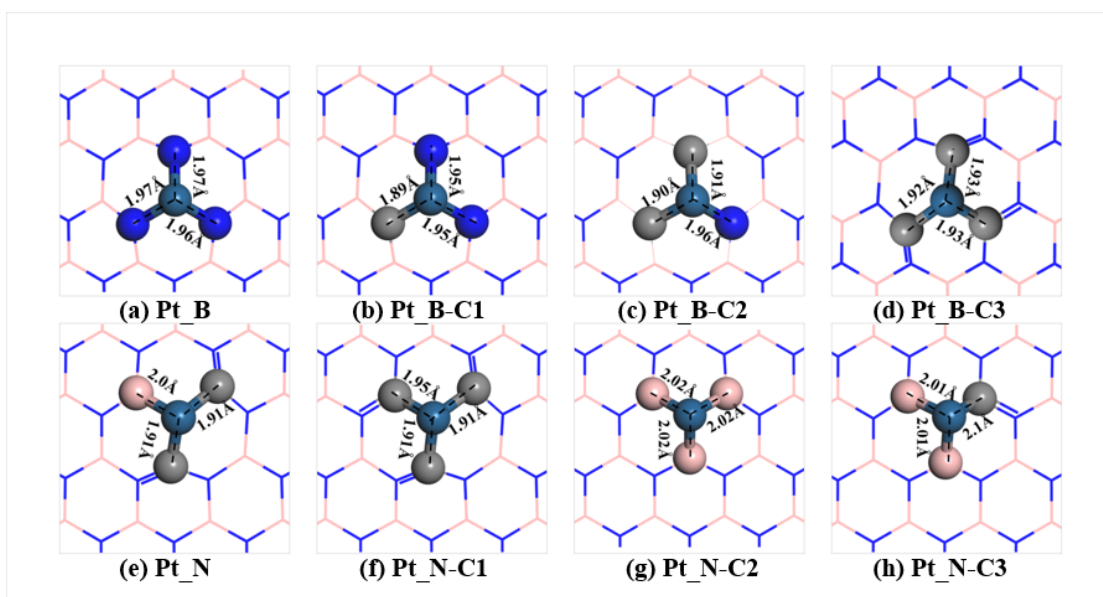


**Figure S1.** Optimized geometric structures of the Pt/V<sub>B</sub> and Pt/V<sub>N</sub> series single-atom catalyst models. Bond lengths are given in angstroms (Å). Blue, pink, gray, and light teal spheres represent nitrogen, boron, carbon, and platinum atoms, respectively.

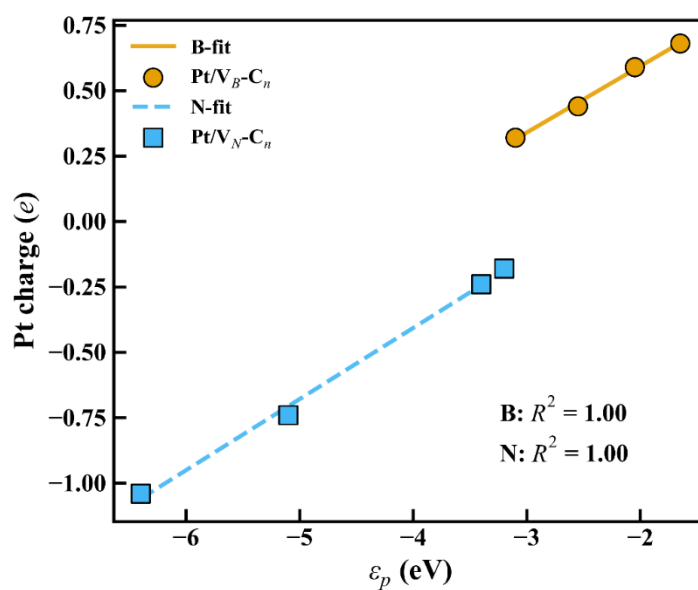


**Figure S2.** Correlation between the Bader charge of the Pt single atom the center-of-mass energy of the p orbital of the adjacent atom ( $\epsilon_p$ ).

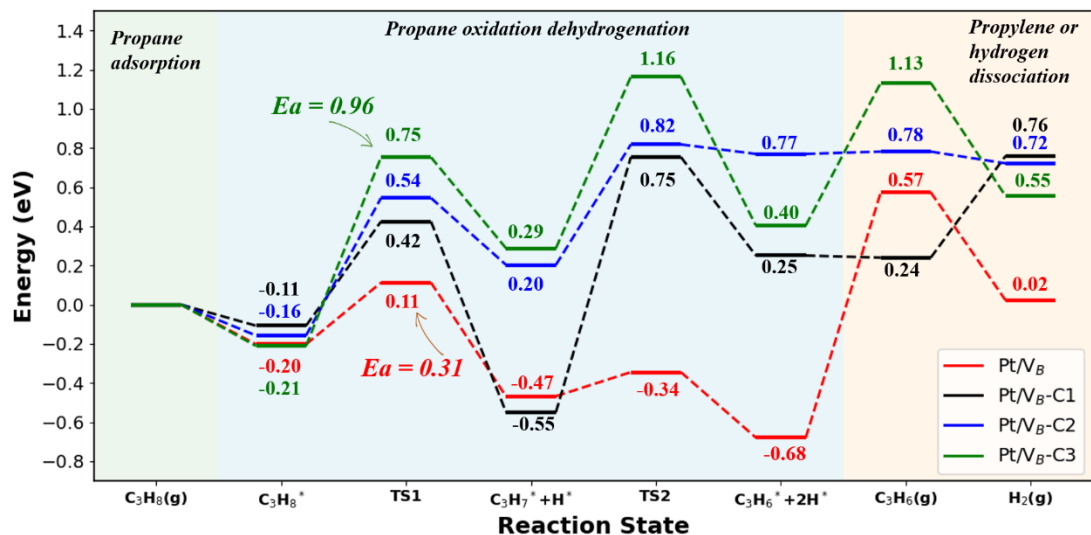


**Figure S3.** Calculated energy pathways for propane dehydrogenation on the Pt/V<sub>B</sub> series catalysts. Energies are relative to the gas-phase propane molecule and the clean catalyst surface. TS1 and TS2 denote the transition states for the first and second C-H bond cleavage, respectively.

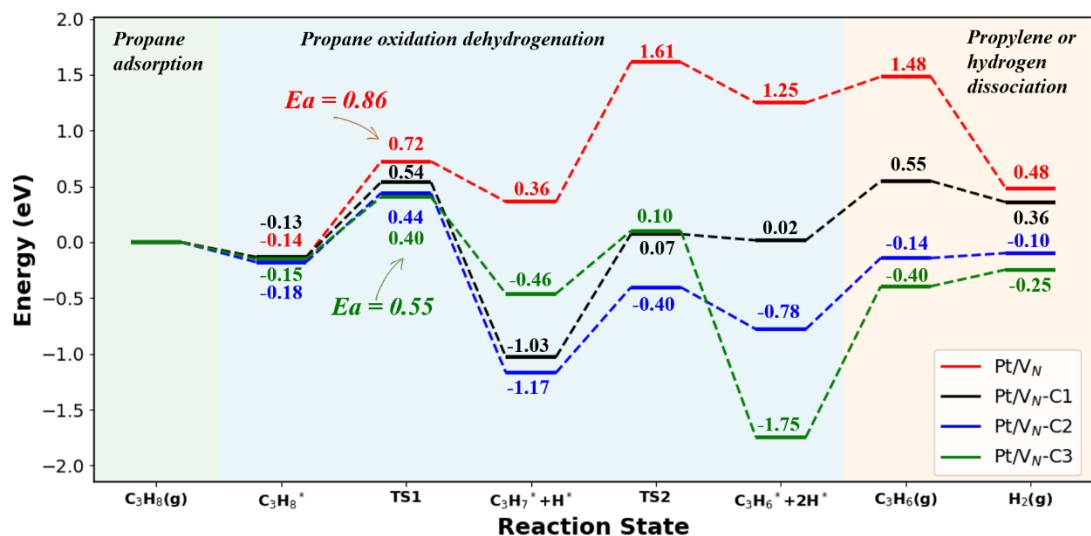


**Figure S4.** Calculated energy pathways for propane dehydrogenation on the Pt/V<sub>N</sub> series catalysts. Energies are relative to the gas-phase propane molecule and the clean catalyst surface. TS1 and TS2 denote the transition states for the first and second C-H bond cleavage, respectively.

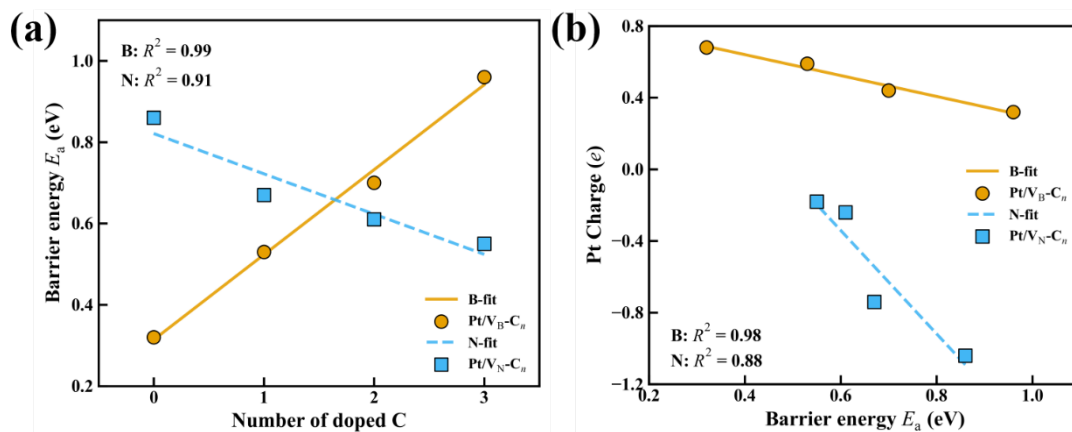


**Figure S5.** (a) Relationship between the barrier energy of the first C-H bond cleavage ( $E_a$ ) and the number of coordinating carbon atoms ( $n$ ). (b) Correlation between the barrier energy of the first C-H bond cleavage ( $E_a$ ) and Bader charge of the Pt single atom

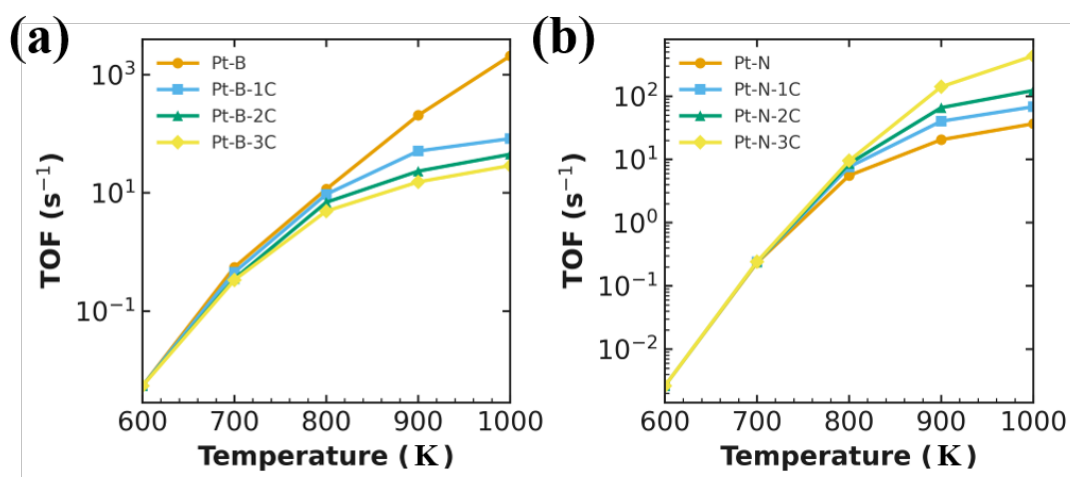


**Figure S6.** (a) Arrhenius plots showing the temperature dependence of the turnover frequency (TOF) for the Pt/ $V_B$  series catalysts at a constant pressure of 1 bar. (b) Arrhenius plots showing the temperature dependence of the turnover frequency (TOF) for the Pt/ $V_N$  series catalysts at a constant pressure of 1 bar.

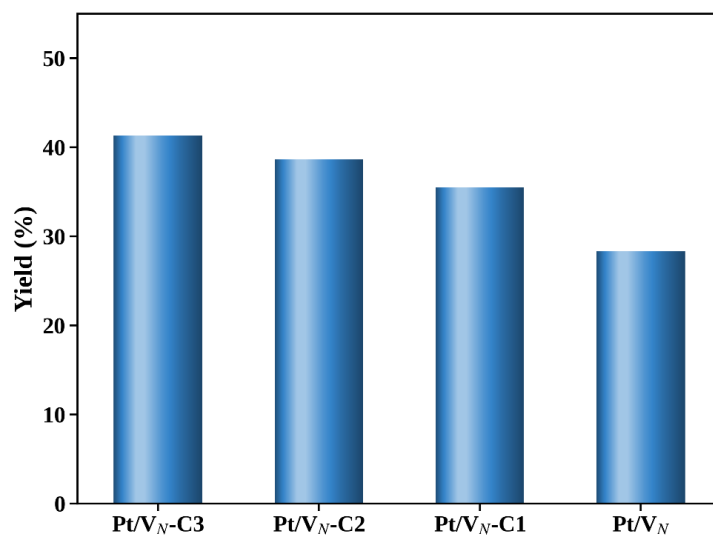


**Figure S7.** Plug-flow reactor predictions (Cantera, 800 K and 1 bar) comparison of Pt/V<sub>N</sub>, Pt/V<sub>N</sub>-C1, Pt/V<sub>N</sub>-C2 and Pt/V<sub>N</sub>-C3: propylene yield bar chart.

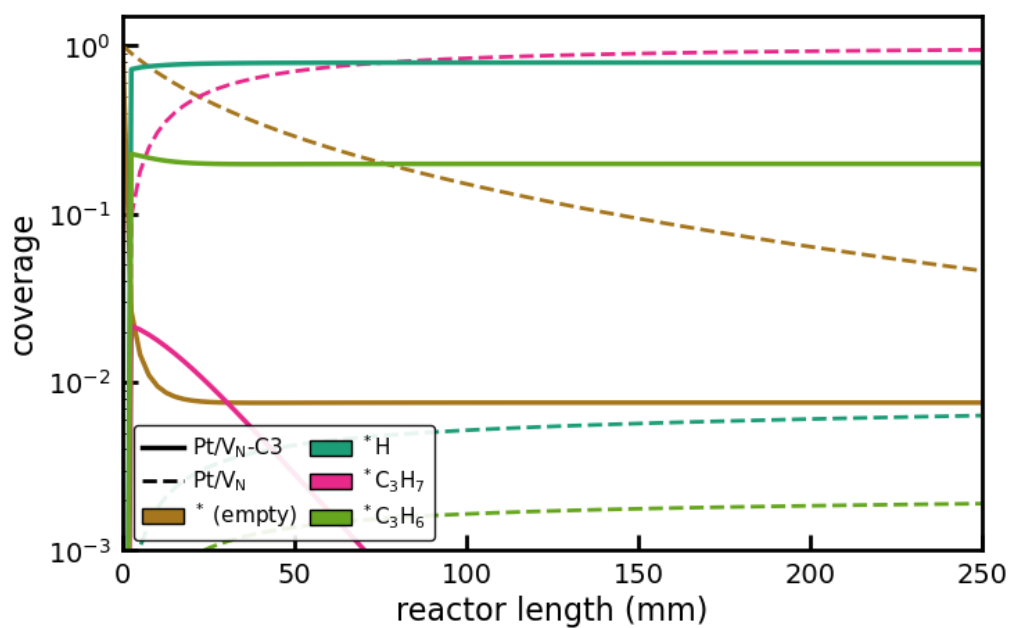


**Figure S8.** Cantera plug-flow simulation at 800 K and 1 bar comparing Pt/V<sub>N</sub>: solid lines and Pt/V<sub>N</sub>-C3: dashed lines: Corresponding surface coverages of vacant sites and key intermediates as functions of reactor length.

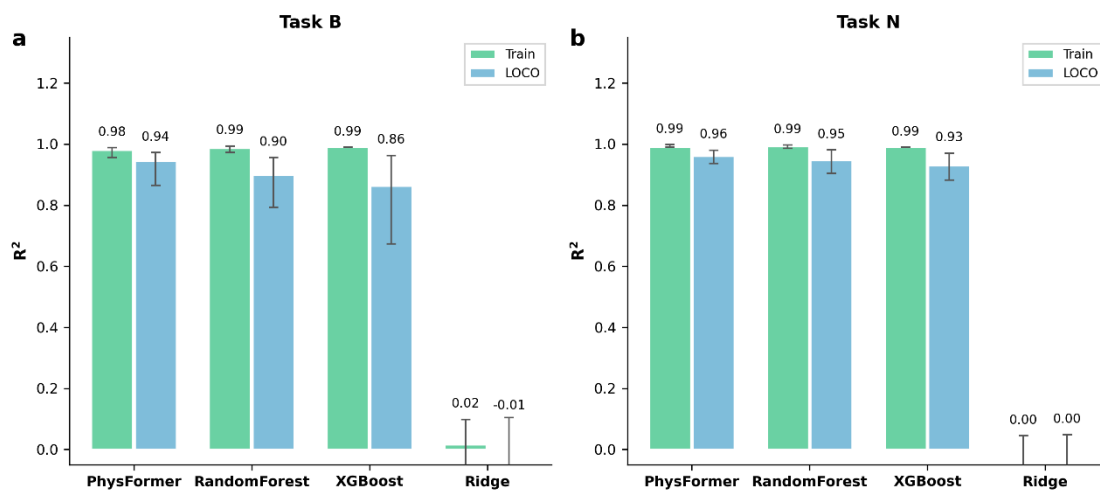


**Figure S9.** Model performance comparison for Pt/V<sub>B</sub> and Pt/V<sub>N</sub> series. Training (green) and leave-one-out cross-validation (blue) R<sup>2</sup> values across four models. PhysFormer achieves the best generalization performance (LOCO R<sup>2</sup> = 0.94–0.96) with minimal overfitting, outperforming tree-based ensembles and linear baselines.

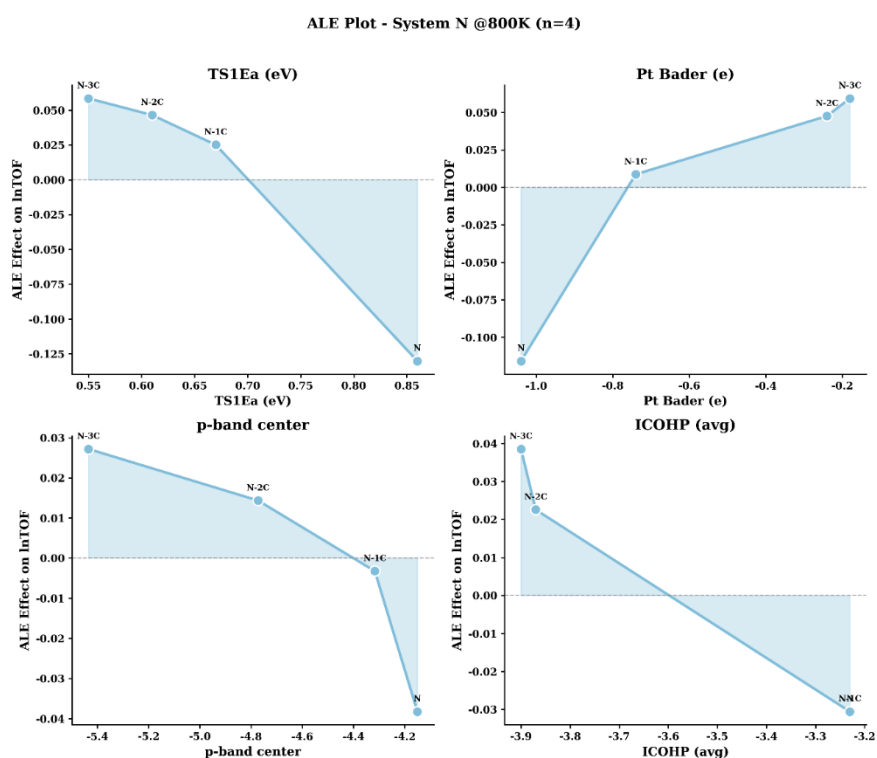


**Figure S10.** Accumulated local effects (ALE) analysis of the PhysFormer model for the Pt/V<sub>B</sub> series at 800 K.

ALE Plot - System B @800K (n=4)

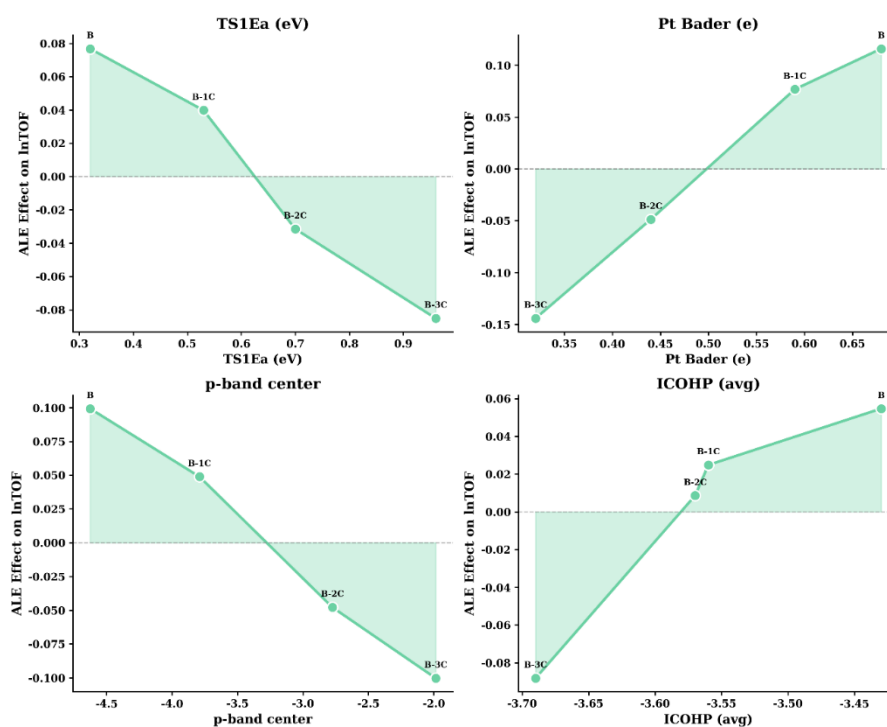


**Figure S11.** Accumulated local effects (ALE) analysis of the PhysFormer model for the Pt/V<sub>N</sub> series at 800 K.

## S1. PhysFormer Physical Constraint Design

To ensure physical plausibility of temperature response, this work imposes a sign constraint on the slope head  $b(\mathbf{x})$ :

$$b(\mathbf{x}) = -\text{softplus}(b_{\text{raw}})$$

This transformation enforces  $b(\mathbf{x}) < 0$ , ensuring that predicted values change monotonically with the inverse temperature variable  $\tilde{u} = 1/T$ , structurally avoiding non-physical phenomena such as temperature trend reversal under small-sample conditions.

Considering that real catalytic systems may deviate from ideal Arrhenius behavior (due to factors such as diffusion limitations, competitive adsorption, etc.), the model introduces a discrete temperature bias term  $g(T)$  with a ‘‘cumulative increment’’ monotonic parameterization design: using the lowest temperature point (600 K) bias as zero baseline, biases for remaining temperature points are generated by cumulative summation of 4 non-negative increments (constrained by softplus):

$$g(T_k) = \sum_{i=1}^k \text{softplus}(\delta_i), \quad k = 1, 2, 3, 4; \quad g(T_0) = 0$$

This design absorbs systematic temperature deviations while maintaining overall monotonic trends, and reduces non-identifiability between the baseline head  $a(\mathbf{x})$  and temperature bias term. Whether to enable the temperature bias module is automatically determined through LOCO cross-validation.

## S2. Hyperparameter Search Space

To ensure fair comparison, all models undergo hyperparameter optimization via LOCO-based grid search. Table S2 lists the search space and optimal configuration for each model.

## S3. PhysFormer Network Architecture and Training Details

PhysFormer is built upon a multilayer perceptron (MLP), with each Trunk network layer containing Linear, LayerNorm, GELU, and Dropout modules. Input dimension is 4 (TS1Ea, Pt Bader charge, p-band center, ICOHP average), outputting to a dual-head structure. Additionally, a wide branch is introduced to establish direct linear connections from raw input, enhancing fitting capability for simple relationships.

Training employs Huber loss ( $\beta = 0.5$ ), which is more robust to outliers compared to MSE. The optimizer is AdamW, combined with early stopping strategy (patience = 200 epochs, maximum 2000 epochs). Gradient clipping threshold is 1.0. Input descriptors are standardized and truncated to  $\pm 4$  standard deviation range. The inverse temperature variable is normalized with 600 K as the reference point.

#### S4. Reliability Validation of PhysFormer under Small-Sample Conditions

To evaluate the generalization capability of PhysFormer under small-sample conditions, we employed a Leave-One-Catalyst-Out (LOCO) cross-validation strategy on a dataset of only 20 samples (4 catalysts  $\times$  5 temperatures). PhysFormer was systematically compared with XGBoost, RandomForest, and Ridge regression, and 95% confidence intervals were estimated via 1,000 bootstrap resamples.

In the Pt/V<sub>B</sub> series, PhysFormer achieved a LOCO test  $R^2$  of 0.94 (95% CI: [0.87, 0.97]), outperforming RandomForest (0.90, CI: [0.79, 0.95]) and XGBoost (0.86, CI: [0.67, 0.96]). In the Pt/V<sub>N</sub> series, PhysFormer again ranked highest with a LOCO test  $R^2$  of 0.96 (95% CI: [0.94, 0.98]), surpassing RandomForest (0.95, CI: [0.90, 0.98]) and XGBoost (0.93, CI: [0.88, 0.97]). Ridge regression failed to produce meaningful fits in either series ( $R^2 \approx 0$ ).

Notably, PhysFormer not only achieved the highest LOCO  $R^2$  in both series but also exhibited the smallest bootstrap standard deviation (0.029 for Pt/V<sub>B</sub> series; 0.012 for Pt/V<sub>N</sub> series), indicating high prediction stability across different catalyst partitions. In contrast, XGBoost attained a perfect training  $R^2$  of 0.99 yet showed a substantial drop in test  $R^2$  with a considerably wider confidence interval (Pt/V<sub>B</sub> series CI width: 0.29 vs. 0.10 for PhysFormer), exhibiting clear signs of overfitting. The small train-test  $R^2$  gap of PhysFormer ( $\Delta = 0.04$  for Pt/V<sub>B</sub> series;  $\Delta = 0.03$  for Pt/V<sub>N</sub> series) further confirms its strong generalization without severe overfitting under small-sample conditions.

These results demonstrate that, by incorporating physical prior knowledge, PhysFormer achieves accurate and robust predictions under the stringent setting of small-sample, leave-one-catalyst-out validation, significantly outperforming conventional machine-learning approaches.